Published in final edited form as:
J Ultrasound Med. 2013 October ; 32(10): . doi:10.7863/ultra.32.10.1789.

Ultrasound Backscatter Microscopy for Imaging of Oral Carcinoma

Matthew Lam, BS, **Abhijit J. Chaudhari, PhD**, **Yang Sun, PhD**, **Feifei Zhou, BS**, **Allison Dobbie, MD**, **Regina F. Gandour-Edwards, MD**, **Steve P. Tinling, PhD**, **D. Gregory Farwell, MD**, **Wayne L. Monsky, MD, PhD**, **K. Kirk Shung, PhD**, and **Laura Marcu, PhD**
Department of Biomedical Engineering, University of California, Davis, California USA (M.L., Y.S., F.Z., L.M.); Departments of Radiology (A.J.C., W.L.M.), Otolaryngology (A.D., S.P.T., D.G.F.), and Pathology and Laboratory Medicine (R.F.G.-E.), University of California Davis School of Medicine, Sacramento, California USA; Ming Hsieh Department of Electrical Engineering, University of Southern California, Los Angeles, California USA (K.K.S.); and Department of Radiology, University of Washington, Seattle, Washington USA (W.L.M.)

Abstract

Objectives—Ultrasound backscatter microscopy (UBM), or ultrasound biomicroscopy, is a noninvasive, label-free, and ionizing radiation–free technique allowing high-resolution 3-dimensional structural imaging. The goal of this study was to evaluate UBM for resolving anatomic features associated with squamous cell carcinoma of the oral cavity.

Methods—The study was conducted in a hamster buccal pouch model. A carcinogen was topically applied to cheeks of 14 golden Syrian hamsters. Six additional hamsters served as healthy controls. A high-frequency (41 MHz, 6-mm focal depth, lateral and axial resolutions of 65 and 37 μm, respectively) UBM system was used for scanning the oral cavity after 14 weeks of carcinogen application. Histologic analyses were conducted on scanned regions.

Results—The histologic structure of buccal tissue and microvasculature networks could be visualized from the UBM images. Epithelial and mucosal hypertrophy and neoplastic changes were identified in animals subjected to the carcinogen. In animals with invasive squamous cell carcinoma, lesion development and destruction of the structural integrity of tissue layers were noted.

Conclusions—In this pilot study, UBM generated sufficient contrast for morphologic features associated with oral carcinoma compared to healthy tissue. This modality may present a practical technique for detection of oral neoplasms that is potentially translatable to humans.

Keywords

biomicroscopy; high-frequency ultrasound; oral cancer; oral tissue characterization; squamous cell carcinoma; ultrasound backscatter microscopy

Head and neck squamous cell carcinoma (HNSCC) is the sixth most common cancer worldwide.[1,2] Approximately 37,000 men and women had a new diagnosis of HNSCC in 2011 in the United States.[3] The 5-year survival rate is only 50% to 60%.[1] Most patients with HNSCC typically present with advanced disease in the clinic despite the fact that oral or

Address correspondence to Abhijit J. Chaudhari, PhD, Department of Radiology, University of California Davis School of Medicine, 4860 Y St, Suite 3100, Sacramento, CA 95817. ajchaudhari@ucdavis.edu.

pharyngeal tumors are easily identifiable within the mouth and throat by direct visualization or simple awake endoscopy.[4,5] Given the advanced stage of oral carcinomas at detection, current treatment approaches such as radiotherapy and surgical resection can result in substantial morbidity and impairment of speech, swallowing, taste, and facial appearance.[6] As such, there is an urgent clinical need for techniques that allow for early diagnosis, optimal staging, and restaging and for monitoring responses following therapy for HNSCC.

Ultrasound (US) imaging is one such technique currently used for the diagnosis, assessment, and surgical management of HNSCC.[7–10] The corresponding US probes, typically with 5–15-MHz transducers, provide sufficient imaging penetration depth but are constrained by limited spatial resolution, which may hamper their effectiveness in detecting neoplastic features characteristic of HNSCC such as early invasive growth and disruptions of subepithelial layers and the basement membrane in suspected lesions.

Other imaging modalities such as optical coherence tomography have been developed to overcome the resolution limitations associated with clinical US imaging. Studies in animal models and patients have yielded images of suspicious oral lesions with axial and lateral resolutions of less than 10 μm, allowing for the visualization of individual tissue layers of the oral mucosa. The spatial resolution afforded by optical coherence tomography allows for the detection of precancerous changes such as epithelial dysplasia in addition to the disruption of healthy tissue layers associated with more advanced neoplastic stages. However, optical coherence tomography is limited to a superficial interrogation of tissue surfaces with a maximum penetration depth ranging from 1 to 3 mm, with commercial systems providing a penetration depth of 1.5 mm and an imaging focal depth of 1.0 mm.[11–14]

High-frequency (>20-MHz) ultrasound backscatter microscopy (UBM) systems may show promise for oral cancer detection by producing high-resolution images at a reasonable penetration depth that may better delineate tissue structures. Specifically, with operating frequencies of 40 to 60 MHz, a spatial resolution of less than 0.1 mm and up to 6 mm of depth penetration with reasonable contrast to noise ratios can be obtained from these systems.[15–18] Commercial systems with these characteristics (eg, Vevo series; VisualSonics, Toronto, Ontario, Canada) have also now become readily available.[18] The sizes of the imaging probes of these commercial systems, however, has made their use in oral applications impractical.

Recently, our group built a compact and portable high-frequency (41-MHz) UBM system that uses a single-element transducer.[19] The size and shape of the probe (specifications in “Materials and Methods”) render it suitable for interrogation of oral tissue in vivo in human patients at up to 6 to 7 mm in depth with high axial resolution (<40 μm).[20,21] In this study, we made use of this system to evaluate whether UBM is sensitive to morphologic changes, such as epithelial and mucosal hypertrophy, lesion development, and destruction of the structural integrity of oral tissue layers, occurring during oral carcinoma initiation and progression. We used our UBM system on a hamster buccal pouch model that mimics human pathologic characteristics.[22–24] We provide correlative analyses between the disease status as assessed by tissue histologic analysis and UBM-based imaging findings.

Materials and Methods

Ultrasound Backscatter Microscopy System and Image Reconstruction

The system consists of a customized, concentrically focused 41-MHz US transducer (Ultrasonic Transducer Resource Center, University of Southern California; 6-mm focal depth, 70% bandwidth, 3.75-mm aperture size) shown in Figure 1a fixed on a motorized x-

y-z stage. The transducer was mounted vertically (z direction) above the region of interest and scanned along the horizontal (x–y) plane. The pulse-echo response of our transducer, shown in Figure 1b, provides a summary of its characteristics. The system has measured lateral and axial resolutions of 65 and 37 μm, respectively.[21]

Ultrasound backscatter microscopic images were formed by subtracting the direct current offset from the US radiofrequency data. A bandpass filter with a frequency range of 24 to 75 MHz was used to reduce the high-frequency noise. The Hilbert transform was applied to the filtered radiofrequency signals to detect the envelopes, followed by logarithmic compression. The processed data for each line of sight were displayed as a grayscale B-mode US image showing the reconstruction of a cross section of tissue. The decibel scale was used for representation. Two-dimensional (2D) images were stacked to create a 3-dimensional (3D) volume. A schematic of the UBM system is shown in Figure 1c.

Hamster Model for Oral Lesions

Imaging of oral carcinoma was performed in a hamster buccal pouch model with golden Syrian hamsters (Charles River Laboratories, Wilmington, MA). Topical 9,10-dimethyl 1,2-benzanthracene (DMBA) solution (Sigma Aldrich Corporation, St Louis, MO) applied on the buccal pouch over the course of 14 weeks was used to induce lesions of various developmental disease states for investigation.[24,25] A total of 20 animals were used in the study, with 14 receiving DMBA painting and the remaining 6 receiving no DMBA painting to serve as true healthy controls. Of the animals studied, 3 representative case studies are presented in this article. All experiments in this study were approved by the Institutional Animal Care and Use Committee at the University of California Davis.

Animal Imaging Protocol

For imaging sessions, animals were anesthetized using a combination of 200-mg/kg ketamine and 13-mg/kg xylazine (Lloyd Laboratories, Shenandoah, IA) via an intraperitoneal injection. Once anesthetized, the animals were restrained using a customized head brace fabricated by our group. The cheek pouch was turned outward, and a plastic dish with an open window filled with phosphate-buffered saline for acoustic coupling was placed over the region to be imaged (Figure 1a). The lesions of interest were selected on the basis of visual identification by an otolaryngologist (S.P.T., A.D., or D.G.F.) as suggestive of a neoplasm or healthy tissue. In vivo imaging was conducted with a total scan time for an individual animal (an area of 6.2 × 4.9 mm) of 3 minutes. The limiting factor for image acquisition was the scanning speed (10 mm/s), which was determined by the pulse repetition rate of the transducer (500 Hz) and the lateral step size (20 μm). On completion of the scan, animals were euthanized with an overdose of ketamine delivered intraperitoneally, and the lesions were surgically excised for histologic analysis.

Histologic Analysis and Interpretation

Tissue at and above the dermal layer was surgically excised. Ink markings were drawn on the tissue to preserve the orientation for histologic analysis and for spatial correlation with UBM images. For healthy controls, excised tissue was biopsied en bloc. Suspected oral lesions were biopsied with accompanying epithelial and mucosal tissue layers. All excised tissue was preserved in 10% formalin, embedded in paraffin, and sectioned for hematoxylin-eosin staining. Histologic specimens were interpreted by light microscopy by an anatomic pathologist (R.F.G.-E.), who was blinded to the results of the imaging experiments. Each specimen was assigned 1 of 5 possible grades: normal, hyperplasia, dysplasia, carcinoma in situ, and invasive carcinoma.

Interpretation of UBM Images

Three-dimensional reconstruction of entire imaging volumes were read by an experienced radiologist (W.L.M.). Anatomic features associated with normal and disease states, such as intactness/destruction of buccal tissue layers, thickening/hypertrophy of the squamous epithelial, mucosal, and submucosal tissue layers, the presence of a lesion, disorganization of glandular tissue, necrosis, and tumor stalks, were identified.

Results

In all 6 control animals, healthy tissue structures and microstructures such as vasculature were observed on UBM and confirmed by histologic analysis. Two of these animals served as case examples (cases 1 and 2). Of the 14 hamsters painted with DMBA, 1 failed to develop any oral lesions, and 1 had an adverse reaction to anesthesia before imaging. Of the 12 remaining animals, 3 developed invasive carcinoma based on the histologic analysis. In all of these animals, UBM confirmed the presence of an invasive lesion based on the visualization of disruption and disorganization of normal epithelial, mucosal, and underlying connective tissue layers. Case 3 is a representative example of invasive carcinoma. The remaining 9 animals developed lesions characterized as noncancerous hyperplasia and noncancerous papillomas based on histopathologic analysis. The UBM images confirmed these findings, as all animals retained intact tissue layers and lacked the disruption in the tissue architecture characteristic of oral tumors (not shown). None of the painted animals developed precancerous dysplasia.

Case 1: Characterization of Healthy Epithelial Tissue Layers

The UBM system provided detailed high-resolution images of the underlying tissue structure of the scanned regions in the healthy hamsters. A representative image of a healthy hamster cheek is shown in Figure 2a, which demonstrates the contrast in the tissue provided by UBM. As verified by histologic analysis of the same tissue (Figure 2b), UBM allowed for the differentiation of the mucosa, connective, and muscle tissue layers as independently verified by the radiologist. Fat-containing regions produced a hypoechoic signal typical of UBM, as highlighted by green arrows in Figure 2, a and b. Backscatter from the dense connective tissue and dermis layers was higher,[26] producing the layers with a hyperechoic signal, as indicated by red arrows in Figure 2, a and b. A hypoechoic region inside the highlighted blue box in Figure 2a was also identified as a possible blood vessel by the radiologist (W.L.M.). The hypoechogenicity of blood vessels was attributed to the plastic (acoustic) window of the animal holder in our setup, which most likely reduced blood flow to the imaged area and caused local hemostasis. This UBM finding was spatially corroborated with a blood vessel traveling transversely along the plane of the histologic section, as shown in Figure 2b.

Case 2: Characterization of Tissue Microstructure

The contrast and resolution afforded by our UBM system is further emphasized by its ability to demonstrate intricate tissue structures such as microvasculature. This type of characterization was possible because our animal holder possibly induced local hemostasis, which resulted in a loss of signal from blood vessels. Superficial blood vessels from a normal buccal cheek shown in Figure 3a were physically measured before imaging and had diameters ranging from 0.25 to 0.4 mm, which matched the geometry of vessels found on UBM cross sections later identified by the radiologist (W.L.M.). To depict the course of the vessels, a set of cross-sectional images were segmented (using intensity-based thresholding) and processed to produce the 3D rendering shown in Figure 3b. In all cross sections, the blood vessel lumen appeared hypoechoic, as indicated by red arrows in Figure 3, c–e. We applied an isotropic trilinear filter on the UBM images to improve visualization. No other

averaging or filtering was used. Figure 3c depicts a lateral cross section of the blood vessel lumen, as highlighted in Figure 3b.

Figure 3, d and e, depicts axial cross sections of the same tissue at depths of 0.44 mm (Figure 3, d and c, blue dotted line) and 0.98 mm (Figure 3, e and c, green dotted line) from the tissue surface, respectively. The latter axial cross section located at a depth of 0.98 mm was close to the focal plane of the transducer (the working distance was 4.7 mm in this case) and produced the best image quality. From the UBM images, microvasculature branching from the vessels indicated by red arrows was measured to range from 50 to 70 μm in diameter (Figure 3e). This measurement was anticipated to be smaller than the physical vessel diameters due to speckle.

Case 3: Characterization of an Oral Lesion

Ultrasound backscatter microscopy provided a method for visualizing entire tissue volumes. Figure 4a is an in vivo image of a potential oral carcinoma seen from an everted hamster buccal pouch. The green dotted box marks the region interrogated by UBM, whereas the blue dotted line bisecting the lesion indicates the location where the histologic specimen was taken. Figure 4, b and c, shows 3D representations of the lesion constructed from the UBM images. The angle for displaying the 3D volume in Figure 4b was manipulated to better visualize diagnostic features of the lesion. A hypoechoic region spanning from the lesion into the underlying connective tissue layer, as indicated by a red arrow, was identified as an invasive tumor stalk by the radiologist (W.L.M.). Figure 4c depicts the same tissue volume shown in Figure 4b with two lateral cross sections highlighted in gold and gray. The two cross sections are spaced 300 μm apart, with the gold section highlighting the 2D UBM image shown in Figure 4d and the gray section highlighting the 2D UBM image shown in Figure 4e. The two UBM cross sections reveal two different pathologic states. In Figure 4d, the delineation among tissue layers is indistinguishable, as emphasized in the region enclosed by the yellow dotted box. Such disruption of the tissue architecture is characteristic of invasive carcinomas.[14,27] On the other hand, Figure 4e depicts a lateral cross section of the same lesion spaced 300 μm away from the image in Figure 4d toward the lesion periphery. The yellow dotted box in Figure 4e emphasizes the difference in the tissue layer appearance from the disorganized structure in Figure 4d. The image in Figure 4e shows clear, definable tissue layer boundaries similar to the normal tissue structures shown in Figure 2a. The only indication of possible disease in Figure 4e is the thickening of the superficial epithelial layer, marked by the red asterisk. This feature can be indicative of benign or precancerous growth. A spatially correlated histologic specimen taken from the midline of the lesion in Figure 4f shows squamous cell carcinoma as interpreted by the pathologist (R.F.G.-E.), confirming the radiologic finding of invasive carcinoma in Figure 4d.

Discussion

The results of this study show that UBM has the ability to discern tissue layers based on image contrast in vivo in a nondestructive manner (Figure 2a). This contrast is the result of acoustic backscatter, which is directly proportional to the change in density found in the boundaries between tissue layers. As a result, less dense fat tissue layers appear hypoechoic (black), whereas denser tissue layers such as muscle and connective tissue appear hyperechoic (white) on images.[26] The spatial resolution of UBM allowed for improved discrimination of the tissue layers over currently used 5–15-MHz US probes. This correlation between the UBM signal intensity and tissue provides the ability to match the regions observed on UBM images with tissue layers seen in histologic specimens of normal tissue. The contrast provided by UBM also facilitated the visualization of tissue vasculature as validated by correlation with histologic specimens (Figure 2, a and b). These blood

vessels appear hypoechoic on images, a phenomenon attributed to the plastic (acoustic) window of the animal holder in our setup, which most likely reduced blood flow to the imaged area and caused hemostasis. For high-frequency transducers of the nature we used here, echoes from blood may possess strengths similar to those from the surrounding tissue. In these cases, UBM may be used in conjunction with exogenous contrast agents and Doppler functionality to provide improved contrast for microvasculature and hence angiogenesis and perfusion.[28–34]

In the cases presented here, the maximum observed tumor thickness was only approximately 3 mm, which can be attributed to the fact that the hamster buccal cheek oral mucosa is typically 2 mm.[27] Nonetheless, UBM still leverages a penetration depth of 6 to 7 mm while maintaining a spatial resolution of tens of micrometers. This additional penetration depth may prove valuable in human HNSCC, in which tumors can range in depth from 1 to up to 28 mm. In fact, tumor depths greater than 4 mm have been correlated with greater cancer category upstaging.[35] With deeper tumors associated with higher mortality and morbidity in HNSCC, the penetration depth of UBM may provide additional tools for high-resolution imaging of tumor progression and pathologic characteristics.

The high-resolution UBM images in this study provided a wealth of information through a 3D view of interrogated tissue. For instance, the combination of penetration depth, resolution, and contrast allowed us to trace the path of vasculature in tissue (Figure 3b). These 3D representations allow us to reorient the interrogated tissue, which lends to the improved visualization of tissue structures such as microvasculature (Figure 3e). In oral carcinoma, microvascular density has been shown to correlate with disease aggressiveness and metastatic potential.[36]

The attributes of resolution, contrast, penetration depth, and 3D image reconstruction of UBM can be used for investigation of possible malignancies. Three-dimensional views of entire lesion volumes (Figure 4b) can be manipulated and “dissected” in software to visualize possible invasion of the tumor stalks. This ability may provide a useful guide for surgery.[37] At the same time, individual lateral and axial cross sections from the same 3D volume can provide images of the lesion comparable to histologic sections, as evident by the correlation of tissue features in the UBM image presented in Figure 4d and matching histologic specimen in Figure 4f. Visualizing multiple different cross sections of a lesion provides a means of addressing sampling errors inherent in histopathologic analysis of tissue biopsies. For example, despite being separated by only 300 μm, the two UBM cross sections illustrated in Figure 4, d and e, reveal two very different pathologic states: the former as invasive squamous cell carcinoma and the latter as either benign or precancerous growth. Histologic sections of the tumor periphery 300 μm away from the lesion center may not have yielded the diagnosis of squamous cell carcinoma. In turn, UBM may have potential applications in both providing intrasurgical staging of lesions and guiding biopsy locations for histopathologic analysis.

In terms of UBM as a structural imaging modality, the only indication of precancerous growth we observed was epithelial layer thickening. Unfortunately, epithelial thickening is a nonspecific indicator, which can also be attributed to benign tissue growth.[14,27] Further studies with a larger sample size will need to be conducted to determine the sensitivity and specificity of our UBM system for characterization of precancerous oral lesions. Another potential area of investigation is multimodal coregistered imaging using functional imaging modalities such as fluorescence lifetime imaging and photoacoustic imaging with UBM[20,38] to differentiate precancerous and benign pathologic states. This type of imaging is an active area of research that our group is pursuing.[19,39,40]

Nonetheless, this study shows that UBM is a promising modality with potential diagnostic and clinical applications in HNSCC management. With intraoperative US (5–15 MHz) already used by radiologists and surgeons to help identify tumor margins and guide surgical resection of HNSCC,[7–10] the increased resolution afforded by UBM can augment the existing technical skills and technology used by clinicians for characterization and treatment of oral carcinoma.

In conclusion, to the best of our knowledge, in this study we performed the first evaluation of UBM for interrogation of HNSCC of the oral cavity using a hamster buccal pouch model. This modality visualized normal healthy anatomy in the oral cavity and was able to virtually dissect a given tissue volume to visualize oral carcinoma-associated pathologic characteristics such as destruction of the structural integrity of oral tissue layers and lesions. We conclude that UBM potentially can offer a rapid, label-free, and ionizing radiation–free noninvasive technique for interrogation of oral neoplasms that is translatable to humans.

Acknowledgments

We thank Jonathan Cannata, PhD, for fabrication of the ultrasound backscatter microscopy setup, Jing Liu, PhD, for help with image processing, and Ramsey D. Badawi, PhD, for insightful discussions regarding the clinical utility of the ultrasound backscatter microscopy system. This work was supported by National Institutes of Health grants R21-RR025818 (to Dr Marcu), R01-HL67377 (to Dr Marcu), and R03-EB015099 (to Dr Chaudhari), and the University of California Davis Vision grant (to Dr Chaudhari).

Abbreviations

DMBA	9,10-dimethyl 1,2-benzanthracene
HNSCC	head and neck squamous cell carcinoma
3D	3-dimensional
2D	2-dimensional
UBM	ultrasound backscatter microscopy
US	ultrasound

References

1. Howlader, N.; Noone, A.; Krapcho, M.; Neyman, N.; Aminou, WW. SEER Cancer Statistics Review, 1975–2008. Bethesda, MD: National Cancer Institute; 2011.
2. Upile T, Jerjes W, Sterenborg HJ, et al. Head & neck optical diagnostics: vision of the future of surgery. Head Neck Oncol. 2009; 1:25. [PubMed: 19594907]
3. National Cancer Institute. Oral cancer. National Cancer Institute web-site. 2011. http://www.cancer.gov/cancertopics/types/oral
4. Gourin CG, McAfee WJ, Neyman KM, Howington JW, Podolsky RH, Terris DJ. Effect of comorbidity on quality of life and treatment selection in patients with squamous cell carcinoma of the head and neck. Laryngoscope. 2005; 115:1371–1375. [PubMed: 16094107]
5. Rahman M, Chaturvedi P, Gillenwater AM, Richards-Kortum R. Low-cost, multimodal, portable screening system for early detection of oral cancer. J Biomed Opt. 2008; 13:030502. [PubMed: 18601519]
6. Carvalho AL, Kowalski LP, Agra IM, Pontes E, Campos OD, Pellizzon AC. Treatment results on advanced neck metastasis (N3) from head and neck squamous carcinoma. Otolaryngol Head Neck Surg. 2005; 132:862–868. [PubMed: 15944556]
7. Lodder WL, Teertstra HJ, Tan IB, et al. Tumour thickness in oral cancer using an intra-oral ultrasound probe. Eur Radiol. 2011; 21:98–106. [PubMed: 20680291]

8. Wakasugi-Sato N, Kodama M, Matsuo K, et al. Advanced clinical usefulness of ultrasonography for diseases in oral and maxillofacial regions. Int J Dent. 2010; 2010:639382. [PubMed: 20445749]
9. Ng SY, Songra AK, Hutchison IL. Novel use of ultrasound-guided surface marking of head and neck tumors invading facial skin. Oral Surg Oral Med Oral Pathol Oral Radiol Endod. 2006; 101:499–504. [PubMed: 16545715]
10. Welkoborsky HJ. Ultrasound usage in the head and neck surgeon's office. Curr Opin Otolaryngol Head Neck Surg. 2009; 17:116–121. [PubMed: 19363347]
11. Feldchtein F, Gelikonov V, Iksanov R, et al. In vivo OCT imaging of hard and soft tissue of the oral cavity. Opt Express. 1998; 3:239–250. [PubMed: 19384366]
12. Wilder-Smith P, Lee K, Guo S, et al. In vivo diagnosis of oral dysplasia and malignancy using optical coherence tomography: preliminary studies in 50 patients. Lasers Surg Med. 2009; 41:353–357. [PubMed: 19533765]
13. Tsai MT, Lee CK, Lee HC, et al. Differentiating oral lesions in different carcinogenesis stages with optical coherence tomography. J Biomed Opt. 2009; 14:044028. [PubMed: 19725739]
14. Wilder-Smith P, Hammer-Wilson MJ, Zhang J, et al. In vivo imaging of oral mucositis in an animal model using optical coherence tomography and optical Doppler tomography. Clin Cancer Res. 2007; 13:2449–2454. [PubMed: 17438104]
15. Foster FS, Pavlin CJ, Harasiewicz KA, Christopher DA, Turnbull DH. Advances in ultrasound biomicroscopy. Ultrasound Med Biol. 2000; 26:1–27. [PubMed: 10687788]
16. Greco A, Mancini M, Gargiulo S, et al. Ultrasound biomicroscopy in small animal research: applications in molecular and preclinical imaging. J Biomed Biotechnol. 2012; 2012:519238. [PubMed: 22163379]
17. Semple JL, Gupta AK, From L, Harasiewicz K, Sauder D, Foster F, et al. Does high-frequency (40–60 MHz) ultrasound imaging play a role in the clinical management of cutaneous melanoma? Ann Plast Surg. 1995; 34:599–605. [PubMed: 7661536]
18. Filoux E, Mamou J, Aristizábal O, Ketterling JA. Characterization of the spatial resolution of different high-frequency imaging systems using a novel anechoic-sphere phantom. IEEE Trans Ultrason Ferroelectr Freq Control. 2011; 58:994–1005. [PubMed: 21622055]
19. Sun Y, Park J, Stephens DN, et al. Development of a dual-modal tissue diagnostic system combining time-resolved fluorescence spectroscopy and ultrasonic backscatter microscopy. Rev Sci Instrum. 2009; 80:065104. [PubMed: 19566223]
20. Sun Y, Chaudhari AJ, Lam M, et al. Multimodal characterization of compositional, structural and functional features of human atherosclerotic plaques. Biomed Opt Express. 2011; 2:2288–2298. [PubMed: 21833365]
21. Sun, Y.; Phipps, J.; Lam, M., et al. Characterization of atherosclerotic plaques using combined time-resolved fluorescence spectroscopy and ultrasonic backscatter microscopy. Paper presented at: SPIE Photonics West; January 22–27, 2011; San Francisco, CA.
22. Gimenez Conti IB, Slaga TJ. The hamster cheek pouch carcinogenesis model. J Cell Biochem. 1993; 53:83–90.
23. Salley J. Experimental carcinogenesis in the cheek pouch of the Syrian hamster. J Dent Res. 1954; 33:253–262. [PubMed: 13152263]
24. Shklar G. Experimental oral pathology in the Syrian hamster. Prog Exp Tumor Res. 1972; 16:518–538. [PubMed: 4557243]
25. Meier JD, Enepekides DJ, Poirier B, Bradley CA, Albala JS, Farwell DG. Treatment with 1-alpha, 25-dihydroxyvitamin D3 (vitamin D3) to inhibit carcinogenesis in the hamster buccal pouch model. Arch Otolaryngol Head Neck Surg. 2007; 133:1149–1152. [PubMed: 18025321]
26. Raju BI, Srinivasan MA. High-frequency ultrasonic attenuation and backscatter coefficients of in vivo normal human dermis and subcutaneous fat. Ultrasound Med Biol. 2001; 27:1543–1556. [PubMed: 11750754]
27. Wilder-Smith P, Jung WG, Brenner M, et al. In vivo optical coherence tomography for the diagnosis of oral malignancy. Lasers Surg Med. 2004; 35:269–275. [PubMed: 15493024]
28. Foster FS, Burns PN, Simpson DH, Wilson SR, Christopher DA, Goertz DE. Ultrasound for the visualization and quantification of tumor microcirculation. Cancer Metastasis Rev. 2000; 19:131–138. [PubMed: 11191052]

29. Goertz DE, Christopher DA, Yu JL, Kerbel RS, Burns PN, Foster FS. High-frequency color flow imaging of the microcirculation. Ultrasound Med Biol. 2000; 26:63–71. [PubMed: 10687794]
30. Foster FS, Zhang MY, Zhou YQ, et al. A new ultrasound instrument for in vivo microimaging of mice. Ultrasound Med Biol. 2002; 28:1165–1172. [PubMed: 12401387]
31. Yeh CK, Ferrara KW, Kruse DE. High-resolution functional vascular assessment with ultrasound. IEEE Trans Med Imaging. 2004; 23:1263–1275. [PubMed: 15493694]
32. Greis C. Ultrasound contrast agents as markers of vascularity and microcirculation. Clin Hemorheol Microcirc. 2009; 43:1–9. [PubMed: 19713597]
33. Qin S, Caskey CF, Ferrara KW. Ultrasound contrast microbubbles in imaging and therapy: physical principles and engineering. Phys Med Biol. 2009; 54:R27–R57. [PubMed: 19229096]
34. Gessner R, Dayton PA. Advances in molecular imaging with ultrasound. Mol Imaging. 2010; 9:117–127. [PubMed: 20487678]
35. Alkureishi LWT, Ross GL, Shoaib T, et al. Does tumor depth affect nodal upstaging in squamous cell carcinoma of the head and neck? Laryngoscope. 2008; 118:629–634. [PubMed: 18094651]
36. Riedel F, Götte K, Bergler W, Rojas W, Hörmann K. Expression of basic fibroblast growth factor protein and its down-regulation by interferons in head and neck cancer. Head Neck. 2000; 22:183–189. [PubMed: 10679908]
37. Ryu J, Park WS, Jung YS. Exclusive endoscopic resection of nasopharyngeal papillary adenocarcinoma via combined transnasal and transoral approach. Clin Exp Otorhinolaryngol. 2010; 6:48–51. [PubMed: 23526700]
38. Wang LV. Prospects of photoacoustic tomography. Med Phys. 2008; 35:5758–5767. [PubMed: 19175133]
39. Sun Y, Hatami N, Yee M, et al. Fluorescence lifetime imaging microscopy for brain tumor image-guided surgery. J Biomed Opt. 2010; 15:056022. [PubMed: 21054116]
40. Sun Y, Xie H, Liu J, et al. In vivo validation of a bimodal technique combining time-resolved fluorescence spectroscopy and ultrasonic backscatter microscopy for diagnosis of oral carcinoma. J Biomed Opt. 2012; 17:116003. [PubMed: 23117798]

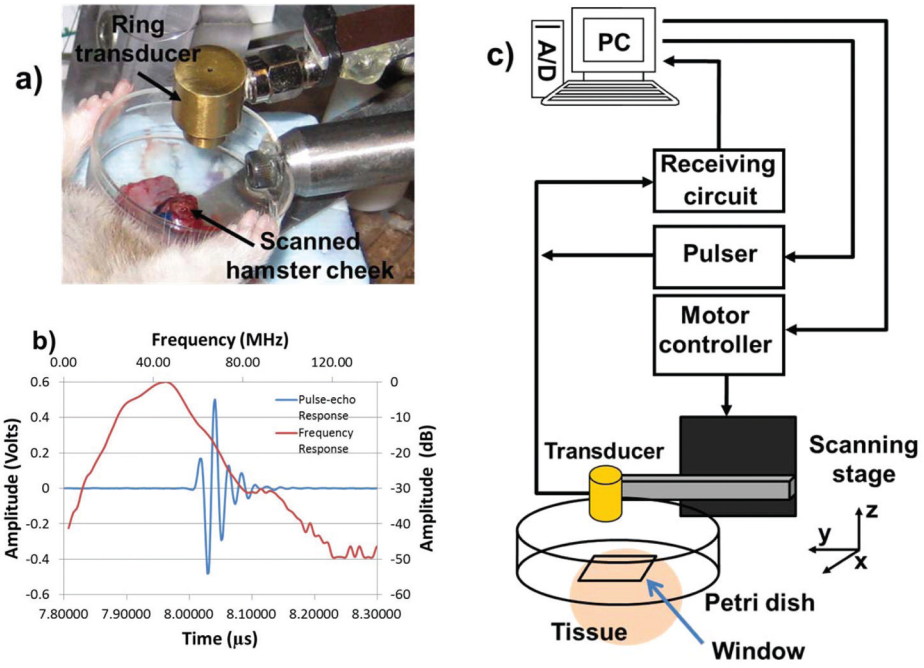

Figure 1.

a, Focused concentric UBM transducer used in the experiment with the clamp used to hold the outwardly turned hamster buccal pouch. A plastic dish with an open window to access tissue was filled with saline for acoustic coupling. **b**, Time domain pulse-echo response and normalized frequency spectrum for the transducer used in the imaging studies. The center frequency of the transducer measured 41 MHz. **c**, Schematic representation of the UBM system. A desktop computer (PC) was used to control both the motorized stage and acquisition of UBM images. A/D indicates analog-to-digital converter.

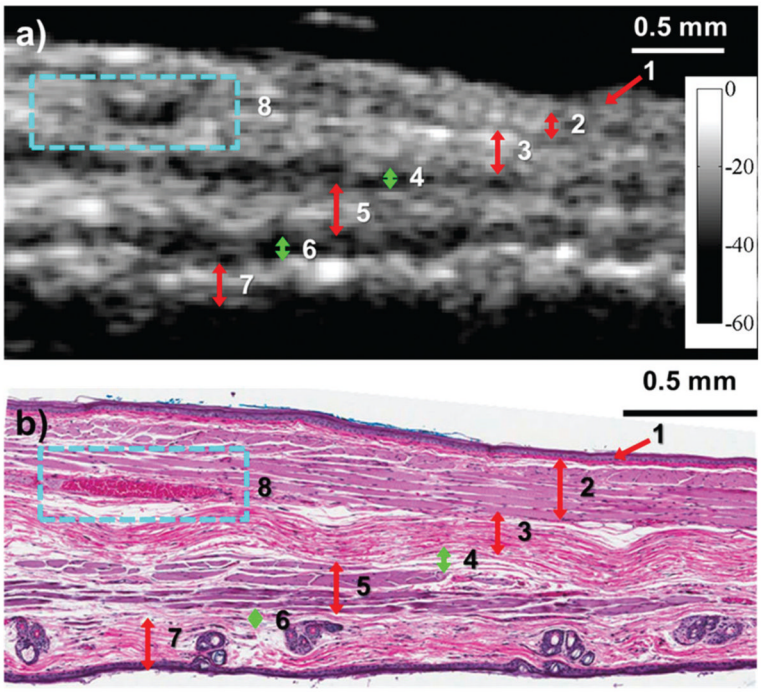

Figure 2.

a, Ultrasound backscatter microscopic image showing a cross section of healthy hamster buccal tissue. The contrast in the UBM image was sufficient for the radiologist to identify the following tissue layers or features: 1, mucosa; 2, skeletal muscle; 3, dense connective tissue; 4, connective tissue with fat (hypoechoic on UBM); 5, skeletal muscle; 6, fat between the muscle and the dermis (hypoechoic on UBM); 7, dermis; and 8, blood vessel. The color bar indicates values on the decibel scale. **b**, Corresponding hematoxylin-eosin–stained specimen of healthy hamster oral mucosa. The blue dotted box indicates the blood vessel. The smaller size of the histologic sample can be attributed to shrinkage that occurs during the extraction and fixation process.

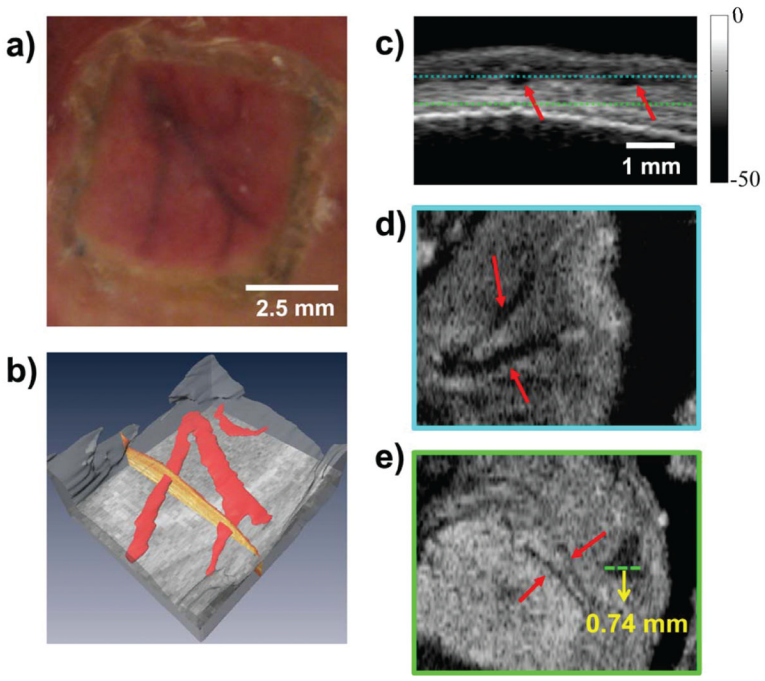

Figure 3.

a, Superficial vasculature in the hamster oral mucosa. **b**, Three-dimensional rendering of the superficial vasculature generated from the UBM image. The course of blood vessels is traced in red. **c**, B-mode grayscale UBM image section from 3D data showing the two blood vessels (red arrows). The blue and green dotted lines indicate the locations of the axial cross sections shown in **d** and **e**, respectively. The two axial cross-sections through the data show two deeper blood vessels, as indicated by red arrows. The intensity and scale bars provided apply to **c**–**e**. The distance of the tissue surface from the transducer was 4.7 mm. **d**, Superficial blood vessels (depth in tissue, 0.44 mm). **e**, Deeper blood vessels (depth in tissue, 0.98 mm). Diameters of the microvasculature indicated in red measured 50 to 70 μm from the UBM image. Contrast for microvasculature was a possible byproduct of our animal holder, which may have induced local hemostasis that resulted in a loss of signal from blood vessels.

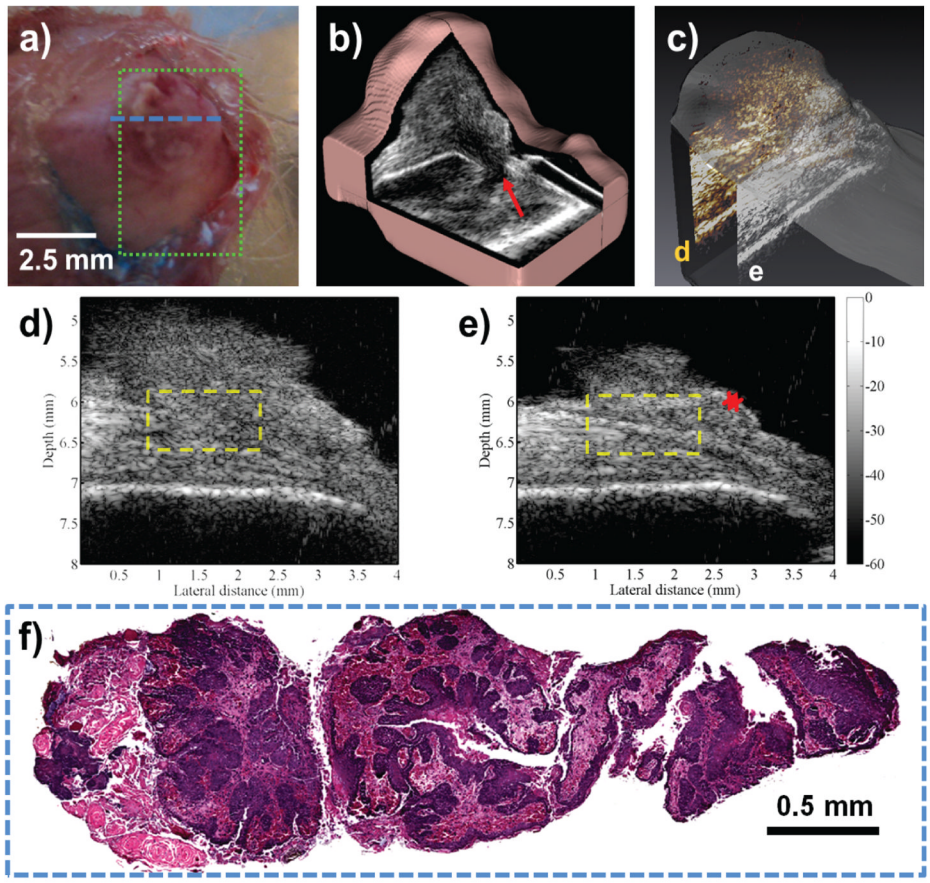

Figure 4.

a, Suspected oral lesion. The green dotted box indicates the region of interest for imaging, and the blue dotted line indicates the location of the histologic specimen shown in **f. b**, Three-dimensional reconstruction of the suspected oral lesion, with the red arrow highlighting a hypoechoic region representative of the tumor stalk. **c**, Three-dimensional representation of the lesion indicating the relative positions of the cross sections shown in **d** (yellow) and **e** (white) relative to each other in the tumor volume. **d**, Single UBM cross section of the tumor closer to the tumor center showing invasion of the lesion through tissue layers. Note the disruption of tissue layer organization (yellow dotted box). **e**, Another UBM cross section from the periphery of the same oral lesion. Preservation of the underlying tissue layer organization (yellow dotted box) and thickening of the epithelial layers (red asterisk) suggest an early stage or a benign lesion. **f**, Hematoxylin-eosin stained biopsy specimen (original magnification ×20) of the oral lesion with squamous cell carcinoma, taken at the center of the tumor, as indicated by the blue dotted line in **a**.